INTERNATIONAL
ENDODONTIC JOURNAL

doi:10.1111/iej.12789

Zirconium oxide and niobium oxide used as radiopacifiers in a calcium silicate-based material stimulate fibroblast proliferation and collagen formation

G. F. Silva[1], J. M. Guerreiro-Tanomaru[1], T. S. da Fonseca[1], M. I. B. Bernardi[2], E. Sasso-Cerri[3], M. Tanomaru-Filho[1] & P. S. Cerri[3]

[1]Department of Restorative Dentistry, School of Dentistry, São Paulo State University (UNESP), Araraquara; [2]Grupo Crescimento de Cristais e Materiais Cerâmicos, Physics Institute of São Carlos, University of São Paulo (USP), São Carlos; and [3]Laboratory of Histology and Embryology, Department of Morphology, School of Dentistry, São Paulo State University (UNESP), Araraquara, Brazil

Abstract

Silva GF, Guerreiro-Tanomaru JM, da Fonseca TS, Bernardi MIB, Sasso-Cerri E, Tanomaru-Filho M, Cerri PS. Zirconium oxide and niobium oxide used as radiopacifiers in a calcium silicate-based material stimulate fibroblast proliferation and collagen formation. *International Endodontic Journal*, **50**, e95–e108, 2017.

Aim To evaluate the influence of the addition of microparticulate (micro) and nanoparticulate (nano) zirconium oxide (ZrO_2) and niobium pentoxide (Nb_2O_5) to a calcium silicate-based cement (CS) on the subcutaneous healing process in rats compared with MTA Angelus™.

Methodology In each rat, two polyethylene tubes filled with the following materials: (i) MTA; (ii) CS + ZrO_2micro; (iii) CS + ZrO_2nano; (iv) CS + Nb_2O_5micro or (v) CS + Nb_2O_5nano were implanted subcutaneously; empty polyethylene tubes were used in the Control group. After 7, 15, 30 and 60 days, the specimens ($n = 5$ per group in each period) were fixed and embedded in paraffin. Masson's trichrome sections were used to obtain the volume density of the inflammatory cells (VvIC) and fibroblasts (VvFb). The sections were also stained with Picrosirius-red to calculate the birefringent collagen content. Fibroblast growth factor-1 (FGF-1) was detected by immunohistochemistry, and the number of immunolabelled cells was obtained. The data were subjected to two-way ANOVA followed by Tukey's test ($P \leq 0.05$).

Results At all periods, the VvIC was significantly lower ($P < 0.001$) in all the CS and Control groups than in the MTA group. At all periods, the VvFb was reduced significantly ($P = 0.023$) in the MTA group in comparison with the other groups. In addition, the number of immunolabelled cells in the capsules of the CS groups was significantly higher ($P < 0.001$) than in the MTA group at all time-points.

Conclusions The experimental materials (CS + ZrO_2 and CS + Nb_2O_5) induced fibroblast proliferation and accelerated the regression of the inflammatory reaction. However, the addition of nanoparticulate radiopacifiers did not improve the biological properties of a calcium silicate-based cement when compared to microparticulate agents.

Keywords: biocompatibility, calcium silicate cement, fibroblast growth factor-1, immunohistochemistry, radiopacifiers.

Received 23 September 2016; accepted 27 April 2017

Correspondence: Paulo Sérgio Cerri, Laboratory of Histology and Embryology, Department of Morphology, School of Dentistry, São Paulo State University (UNESP), Araraquara, Rua Humaitá, 1680, Centro, CEP 14801–903, Araraquara, SP, Brazil (e-mail: pcerri@foar.unesp.br).

Introduction

Tricalcium silicate-based cements (CS), including Mineral Trioxide Aggregate (MTA), are composed primarily of tricalcium silicate, dicalcium silicate, and

tricalcium aluminate (Camilleri *et al.* 2005). CS has been widely used in dental applications due to its advantages in comparison with other materials (Mitchell *et al.* 1999, Parirokh & Torabinejad 2010, da Silva *et al.* 2011, Gandolfi *et al.* 2015). However, bismuth oxide (Bi_2O_3), a radiopacifier agent that is added to commercial MTA, decreases its compressive strength (Coomaraswamy *et al.* 2007, Camilleri 2008) and promotes tooth discoloration (Marciano *et al.* 2015, Marconyak *et al.* 2016). Moreover, bismuth oxide inhibits cell proliferation, suggesting that this substance has a toxic effect (Camilleri *et al.* 2004). Due to these disadvantages, other radiopacifying agents have been added to CS in attempt to improve its biocompatibility (Bortoluzzi *et al.* 2009, Hungaro Duarte *et al.* 2012, Viola *et al.* 2012). Zirconium oxide (ZrO_2) and niobium oxide (Nb_2O_5) mixed with CS have given satisfactory results and are considered an alternative radiopacifier to Bi_2O_3 (Silva *et al.* 2014, 2015, Viapiana *et al.* 2014). ZrO_2 does not affect the properties of Portland cement, such as the pH and setting time (Camilleri *et al.* 2011, Cutajar *et al.* 2011). Recently, it was demonstrated that the addition of microparticulate or nanoparticulate zirconium oxide to Portland cement yielded a CS with a higher compressive strength and a lower inflammatory reaction in tissues than when the Bi_2O_3 was added to CS (Silva *et al.* 2014). Furthermore, there is evidence that the use of ZrO_2 instead of Bi_2O_3 reduces tooth discoloration (Marciano *et al.* 2015, Marconyak *et al.* 2016).

Some studies have shown that the addition of Nb_2O_5 to Portland cement increases its initial time setting, and the solution containing this experimental material exhibits a high alkaline pH (Silva *et al.* 2015). Nb_2O_5 improves the microhardness of materials (Leitune *et al.* 2013), and when added to CS, it has an adequate radiopacity (Guerreiro-Tanomaru *et al.* 2014, Silva *et al.* 2015).

An *in vitro* study using osteoblast-lineage cells revealed that the addition of ZrO_2 to root filling materials containing calcium silicate and resin provided greater cell viability and cell proliferation than the addition of Nb_2O_5 (Mestieri *et al.* 2014). However, a significant increase in mineralized nodule deposition was observed in osteoblast cultures with the Nb_2O_5 associated with experimental cements in comparison with MTA Plus® and Biodentine® (Gomes-Cornélio *et al.* 2017).

Studies focusing on the influence of ZrO_2 and Nb_2O_5 associated with CS on the healing process have not been performed. It is known that the recovery of connective tissues in dental and periodontal structures to a healthy condition is a complex process that involves several overlapping cellular and molecular events. The host response to the material chosen plays an important role in the outcome of the endodontic therapy, as the cells produce and release growth factors, cytokines and chemokines, which control the tissue healing process. Amongst several factors, fibroblast growth factor-1 (FGF-1) participates in tissue remodelling, promoting fibroblast proliferation and migration (Powers *et al.* 2000, Barrientos *et al.* 2008).

The purpose of this study was to evaluate whether the addition of zirconium oxide (ZrO_2) and niobium oxide (Nb_2O_5) to calcium silicate-based material (CS) induces fibroblast proliferation, favouring the replacement of the inflammatory process by dense subcutaneous connective tissue, which is similar to what is observed in the process of periodontal tissue repair. In addition, whether nanoparticles of ZrO_2 and Nb_2O_5 associated with CS interfere with the formation of collagen and stimulate the formation of a subcutaneous fibrous capsule in the rat was also evaluated. The null hypothesis was that ZrO_2 and Nb_2O_5 when associated with a calcium silicate-based material would not induce the formation of collagen fibres in the capsules.

Materials and methods

Experimental procedure

Sixty adult male Holtzman rats (*Rattus norvegicus albinus*) weighing 250 ± 10 g were maintained in individual stainless steel cages under a 12:12-h light-dark cycle at a controlled temperature (23 ± 2 °C) and humidity (55 ± 10%) and with food and water provided *ad libitum*. The research protocol on the animal use in this study was authorized by the Ethical Committee for Animal Research of the São Paulo State University, Brazil (Araraquara Dental School-UNESP).

Experimental proceedings were performed as recommended by the ISO standards (ISO-10993-6 2007). One hundred and twenty polyethylene tubes were implanted on 60 rats, each with two tubes; empty tubes were used as Controls. Polyethylene tubes with a 10.0 mm length and a 1.6 mm diameter (Embramed Indústria Comércio, São Paulo, SP, Brazil) previously sterilized with ethylene oxide were filled with the following materials: (i) mineral trioxide

aggregate (white MTA – Angelus, Londrina, PR, Brazil); (ii) 70% calcium silicate-based (CS) cement (white Portland cement; CPB-40, Votorantin Cimentos, Camargo Correa S.A., Pedro Leopoldo, MG, Brazil) with 30% microparticulated zirconium oxide (ZrO_2micro; Sigma-Aldrich, St Louis, MO, USA); (iii) 70% CS with 30% nanoparticulate zirconium oxide (ZrO_2nano); (iv) 70% CS with 30% microparticulate niobium pentoxide (Nb_2O_5micro; Sigma-Aldrich) and (v) 70% CS with 30% nanoparticulate niobium pentoxide (Nb_2O_5nano). Each powder had been previously sterilized in ultraviolet light for 30 min. A ratio of 30% ZrO_2 or Nb_2O_5 and 70% CS by weight were used for the analyses. The materials, except for the nanoparticulate products, were mixed at a ratio of 1 g cement powder per 0.3 mL of liquid (distilled water). CS + ZrO_2nano and CS + Nb_2O_5nano were prepared using a powder/liquid mixing ratio of 1 g/0.33 mL (Silva *et al.* 2014, 2015). Nanoparticulate ZrO_2 and Nb_2O_5 were prepared by the polymeric precursor method at the Institute of Physics of São Carlos (University of São Paulo, São Carlos, Brazil), and the particle sizes obtained were 74 and 83 nm, respectively, which was confirmed by a Brunauer–Emmett–Teller (BET) surface area analysis.

According to the materials used, the study was conducted using six groups as follows: the MTA; CS + ZrO_2micro; CS + ZrO_2nano; CS + Nb_2O_5micro; CS + Nb_2O_5nano and Control (empty polyethylene tube) groups. Immediately after the materials were mixed, the polyethylene tubes were filled and implanted into the dorsal area subcutaneously.

The animals were anaesthetized with an intraperitoneal injection of ketamine (80 mg kg^{-1} of body weight) combined with xylazine (4 mg kg^{-1} of body weight). The dorsal skin was shaved and disinfected with a 5% iodine solution. Subsequently, a 20-mm-long incision was made using a No. 15 scalpel (Fibra Cirúrgica, Joinvile, SC, Brazil), and two polyethylene tubes, each filled with one of the materials, were placed into the subcutaneous pocket. After 7, 15, 30 and 60 days of implantation, the tubes and the surrounding connective tissue, that is the capsule, were removed, and the specimens were processed for paraffin embedding. Five subcutaneously implanted polyethylene tubes per group were analysed in each period.

Histological procedures

The specimens were fixed for 48 h at room temperature in 4% formaldehyde (prepared from paraformaldehyde) buffered at pH 7.2 with 0.1 mol L^{-1} sodium phosphate. Subsequently, the specimens were dehydrated in graded concentrations of ethanol, clarified in xylene and embedded in paraffin. From each implant, sixty longitudinal 6-μm-thick sections were collected onto slides; five nonserial sections were stained with Masson's trichrome for morphological evaluation and analysis of the volume density (Vv) of fibroblasts (VvFb) and inflammatory cells (VvIC) in the capsules adjacent to the orifices of the tubes containing the material. For each implant, three nonserial sections were stained with Picrosirius-red to estimate the collagen content. The sections were attached to silanized slides, subjected to immunohistochemistry for the detection of fibroblast growth factor-1 (FGF-1) and quantified by the number of FGF-1 immunolabelled cells.

Volume density (%) of fibroblasts (VvFb) and inflammatory cells (VvIC)

Volume density was undertaken using a light microscope (BX51, Olympus, Tokyo, Japan) and an image analysis system (Image Pro-Express 6.0, Olympus). In five implants from each group per time period, two sections of the capsule at least 150 μm apart were stained with Masson's trichrome and captured at ×695 magnification. Using the image analysis system, a standardized reticular grid containing 204 intersections/points was superimposed on the captured images. The number of points on the fibroblasts and inflammatory cells (neutrophils, lymphocytes, plasma cells and macrophages) was computed; blood vessels, extracellular spaces, collagen fibres and material particles in the capsule were computed as other structures (VvO).

Immunohistochemical detection of FGF-1

For antigen retrieval, the deparaffinized sections were immersed in 0.001 mol L^{-1} sodium citrate buffer pH 6.0, and submitted to microwave oven cycles for 20 min at 90–94 °C. After a cooling-off period, the sections were immersed in 5% hydrogen peroxide for 20 min. After washing in 0.1 mol L^{-1} sodium phosphate buffer (PBS) at pH 7.2, the sections were incubated for 30 min with 2% bovine serum albumin (Sigma-Aldrich Chemie, Munich, Germany). Subsequently, the sections were incubated overnight at 4 °C with the primary mouse antibody anti-FGF-1 (Santa Cruz Biotechnology, Santa Cruz, CA, USA), which was diluted at 1 : 150. After washing in PBS, the immunoreaction was detected by the Labelled Streptavidin-Biotin system (LSAB-plus kit; Dako,

Carpinteria, CA, USA). The sections were incubated for 20 min at room temperature with a multi-link solution containing biotinylated mouse/rabbit/goat antibodies, washed in PBS and incubated with the streptavidin–peroxidase complex for 20 min at room temperature. The peroxidase activity was revealed by Betazoid DAB (Biocare Medical, Concord, CA, USA) for 5 min; the sections were counterstained with Carazzi's haematoxylin. In some sections used as negative controls, the primary antibody incubation step was replaced by incubation in nonimmune serum (Sigma-Aldrich Chemie).

Numerical density of FGF-1-immunolabelled cells

The numerical density of the immunolabelled cells was estimated in all specimens (implants). In each section, a standardized area (0.09 mm^2) was captured using an Olympus camera (DP-71, Tokyo, Japan) attached to a light microscope (BX51, Olympus) at ×695 magnification. The number of immunolabelled cells was computed using an image analysis system (Image Pro-Express 6.0, Olympus). For each implanted tube, the FGF-1-positive cells (brown-yellow colour) were counted in the standardized area and the number of FGF-1-positive cells per mm^2 was obtained (Viola *et al.* 2012, Silva *et al.* 2014, da Fonseca *et al.* 2016).

Polarized light microscopy analysis

For the collagen content estimation of the capsules, the sections were stained with a 0.1% Picrosirius-red solution and were analysed under a light microscope (BX51, Olympus) equipped with filters to provide polarized illumination (Junqueira *et al.* 1979, 1982). In five implants per group in each time period, two Picrosirius-red-stained sections from the capsule adjacent to the materials were captured under polarized light at ×170 magnification; the smallest distance between the sections was 300 μm. In each section, a standardized area (1.45 mm^2) was captured, and a total area of 2.90 mm^2 was evaluated per implant. The birefringent collagen frequency was estimated using the following hue definition: red 2–38 and 230–256, yellow 39–51 and green 52–128 (Manni *et al.* 2011). The collagen content was calculated as a percentage of the area of each image (expressed in pixels) using ImageJ® (NIH) program, as previously described (Rich & Whittaker 2005). The data from each hue (red, yellow and green) were determined and are expressed as the percentage of the total number of collagen pixels, which, in turn is expressed as a percentage of the total number of pixels in the image (Koshimizu *et al.* 2013).

Statistical analysis

Data were analysed using statistical software SigmaStat 2.0 (Jandel Scientific, Sausalito, CA, USA). Two-way analysis of variance (ANOVA) followed by Tukey's multiple comparisons test was used to evaluate differences amongst groups and the differences de each group over time. The significance level accepted was $P \leq 0.05$.

Results

Morphological and quantitative analysis (VvFb and VvIC)

In all the groups, the capsules adjacent to the opening of the polyethylene tubes had few fibroblasts amongst the many inflammatory cells and blood vessel profiles after 7 days (Fig. 1a–f). After 15 days, thin collagen fibres were present amongst the fusiform fibroblasts, whereas the inflammatory cells were often situated in the innermost portion of the capsule, that is adjacent to the opening of the tube. Several blood vessel profiles were observed throughout the capsule in all the groups, except in the Control group; in this group, the capsules had scarce blood vessels and numerous fibroblasts (Fig. 1g–l). In all the groups, after 30 and 60 days, the capsules exhibited several fibroblasts and well-defined bundles of collagen fibres (Fig. 2a–l). Some multinucleated giant cells were also observed in the capsules, mainly on days 7 and 15 (Figs 1a,e,g,k and 2d).

According to Table 1, the quantitative analysis of the capsules revealed a significant increase ($P < 0.001$) in the volume density of the fibroblasts (VvFb) after 15 days compared to 7 days in all the groups.

Figure 1 Light micrographs of sections showing portions of the capsules adjacent to the opening of the subcutaneously implanted tubes (I) after 7 (a–f) and 15 (g–l) days of implantation. (a–l) The capsules show numerous inflammatory cells (arrows) and scarce collagen fibres (in blue). Fb, fibroblasts; Bv, blood vessels; Cf, bundles of collagen fibres; Gc, Giant cells. Masson's trichrome. Bars: 40 μm.

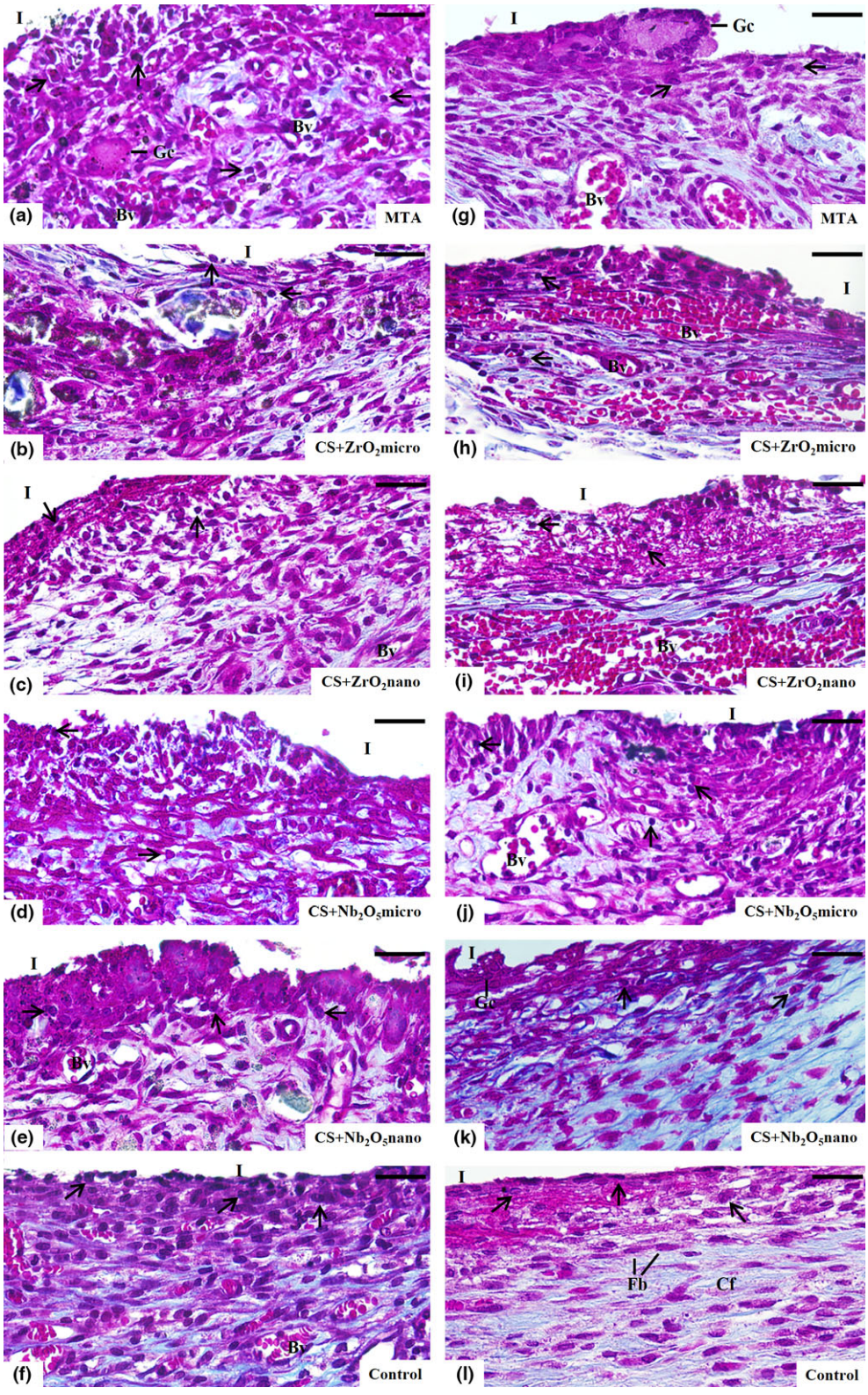
I
Bv
Gc
(a)
MTA
(g)
MTA
(b)
CS+ZrO2micro
(h)
CS+ZrO2micro
(c)
CS+ZrO2nano
(i)
CS+ZrO2nano
(d)
CS+Nb2O5micro
(j)
CS+Nb2O5micro
(e)
CS+Nb2O5nano
(k)
CS+Nb2O5nano
(f)
Control
Fb
Cf
(l)
Control

Significant increase ($P < 0.001$) in the VvFb was verified in the CS + Nb_2O_5micro, CS + Nb_2O_5nano and Control groups at 30 days. From days 15 to 30, significant differences were not observed in the MTA, CS + ZrO_2micro and CS + ZrO_2nano groups. At 60 days, a significant increase ($P < 0.001$) in the VvFb was found in all the groups. In all the periods, the VvFb was significantly lower ($P = 0.023$) in the MTA group compared with the other groups; otherwise, the VvFb was significantly higher in the Control group. With regard to the incidence of inflammatory cells (VvIC), the highest values were observed after 7 days. In all the groups, a gradual and significant reduction ($P < 0.001$) in the VvIC was verified over time. At all periods, the VvIC was significantly lower ($P < 0.001$) in all the CS groups and Control group compared to the MTA group.

Numerical density of FGF-1-immunolabelled cells

In the sections submitted to immunohistochemistry for FGF-1 detection, immunolabelled cells (brown-yellow colour) were observed in the capsules of all the groups. Accentuated immunolabelling was observed in the capsules after 7 days compared with 60 days (Fig. 3a–l). Fibroblasts and inflammatory cells, mainly lymphocytes, plasma cells, and macrophages, exhibited FGF-1 immunolabelling (Fig. 3a–f). Moreover, immunolabelled mast cells were also observed, particularly in the collagen-rich capsules after 60 days (Fig. 3g–l). In the sections used as negative controls, no immunolabelled cells were found (data not shown).

According to Table 2, the quantitative analysis revealed a significant ($P < 0.001$) and gradual decrease in the numerical density of the FGF-1-immunolabelled cells in the capsules from 7 days to 60. In all the periods, the number of immunolabelled cells in the capsules of the CS + ZrO_2 (micro and nano) and CS + Nb_2O_5 (micro and nano) groups was significantly higher ($P < 0.001$) than in the MTA group, whereas the highest number of FGF-1-positive cells was observed in the Control group. Significant differences ($P = 0.555$) were not detected between the CS + ZrO_2 (micro and nano) and CS + Nb_2O_5 (micro and nano) groups at any time-point, except after 30 days; in this period, the number of immunolabelled cells in the CS + Nb_2O_5nano group was significantly lower ($P < 0.001$) than that of the CS + ZrO_2 (micro and nano) and CS + Nb_2O_5 microgroups.

Birefringent collagen content

After 7 days, the capsules exhibited few and thin birefringent collagen fibres (Fig. 4a-f), whereas thick bundles of birefringent collagen fibres were observed in the capsules after 60 days (Fig. 4g–l). In all the periods, the birefringent collagen content was significantly higher ($P < 0.001$) in the capsules of the CS + ZrO_2 (micro and nano) and CS + Nb_2O_5 (micro and nano) groups than in the capsules of the MTA group; the highest values were found in the Control group capsules. After 60 days, a significant increase ($P = 0.008$) in collagen content was observed in the capsules of all the groups (Table 2).

Discussion

The findings indicate that the association of micro- and nanoparticulate ZrO_2 or Nb_2O_5 with calcium silicate-based cement (CS) induces the proliferation of fibroblasts, which produce a collagen-rich capsule that replaces the inflammatory process. High FGF-1 immunoexpression was accompanied by a reduced number of inflammatory cells, and large number of fibroblasts indicates that this factor participates in the regression of the inflammatory process as well as in fibroblast proliferation. Moreover, CS + ZrO_2 and CS + Nb_2O_5 induced a reduced inflammatory reaction compared to MTA reinforcing the concept that these experimental calcium silicate-based cements are biocompatible (Silva *et al.* 2014, 2015).

In the present study, ZrO_2 and Nb_5O_2 (micro- or nanoparticulate) were used as radiopacifying agents at a ratio of 30% of ZrO_2 or Nb_2O_5 to 70% of CS by weight. There is evidence that the addition of 30% ZrO_2 to the calcium silicate-based cement provides a material with suitable physicochemical properties to

Figure 2 Light micrographs of sections showing portions of the capsules adjacent to the opening of the subcutaneously implanted tubes (I) after 30 (a–f) and 60 (g–l) days of implantation. Typical fibroblasts (Fb) are observed amongst the thick bundles of collagen fibres (Cf) in the capsules; few inflammatory cells (arrows) are observed. In (e) (CS + Nb_2O_5nano), material particles (asterisks) are observed amongst the inflammatory cells and blood vessels (Bv). Gc, giant cell. Masson's trichrome. Bars: 40 μm.

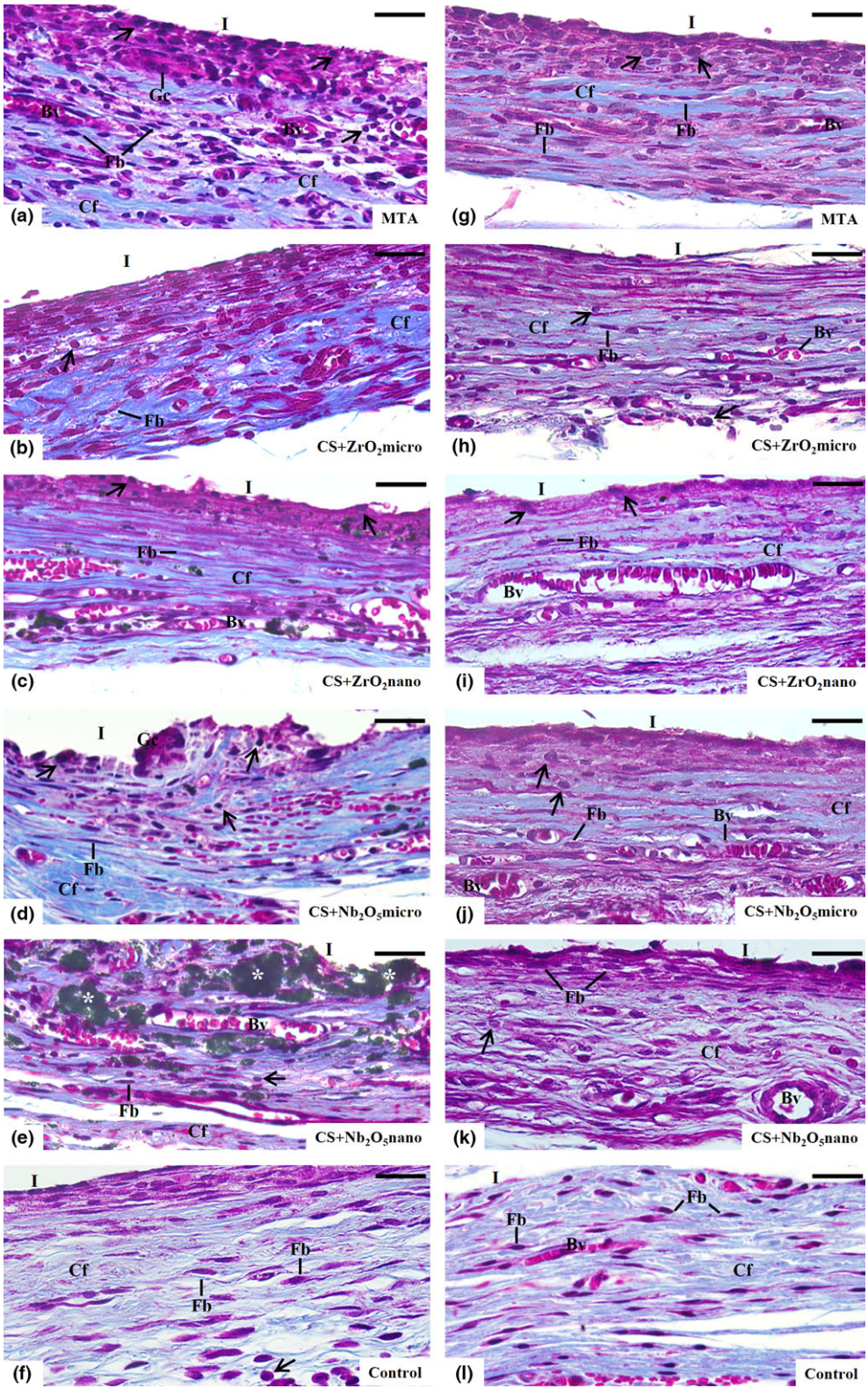
I
Gc
Bv
Fb
Cf
(a) MTA
(g) MTA
(b) CS+ZrO2micro
(h) CS+ZrO2micro
(c) CS+ZrO2nano
(i) CS+ZrO2nano
(d) CS+Nb2O5micro
(j) CS+Nb2O5micro
(e) CS+Nb2O5nano
(k) CS+Nb2O5nano
(f) Control
(l) Control

Table 1 Volume density (%) of the fibroblasts (VvFb), inflammatory cells (VvIC) and other structures (VvO) in the capsules from the groups after 7, 15, 30 and 60 days

	MTA	CS + ZrO_2 micro	CS + ZrO_2 nano	CS + Nb_2O_5 micro	CS + Nb_2O_5 nano	Control
7 days						
VvFb	4.8 (0.4)^{a,1}	6.6 (0.7)^{b,1}	6.6 (1.8)^{b,1}	7.0 (0.5)^{b,1}	6.7 (2.1)^{b,1}	9.3 (0.4)^{c,1}
VvIC	16.0 (0.7)^{a,1}	14.4 (0.7)^{b,1}	14.4 (1.1)^{b,1}	13.9 (1.1)^{b,1}	14.7 (1.4)^{b,1}	7.0 (0.7)^{c,1}
VvO	78.2 (0.4)^{a,1}	79.0 (1.3)^{a,1}	79.0 (2.1)^{a,1}	79.1 (0.7)^{a,1}	78.6 (0.9)^{a,1}	83.7 (3.5)^{a,1}
15 days						
VvFb	10.0 (0.7)^{c,2}	14.0 (2.1)^{b,2}	13.9 (3.5)^{b,2}	14.4 (2.1)^{b,2}	13.5 (2.1)^{b,2}	18.6 (2.8)^{a,2}
VvIC	11.0 (0.7)^{a,2}	6.6 (2.1)^{b,2}	7.0 (2.8)^{b,2}	6.3 (1.4)^{b,2}	7.6 (0.7)^{b,2}	2.4 (0.1)^{c,2}
VvO	79.0 (2.9)^{a,1}	79.4 (2.2)^{a,1}	79.1 (2.4)^{a,1}	79.3 (1.5)^{a,1}	78.9 (2.5)^{a,1}	77.0 (3.1)^{a,1}
30 days						
VvFb	11.0 (0.7)^{a,2}	17.9 (4.9)^{b,2}	18.7 (4.2)^{b,2}	18.1 (1.4)^{b,3}	18.6 (1.4)^{b,3}	20.9 (1.9)^{c,3}
VvIC	6.8 (0.1)^{a,3}	3.1 (0.9)^{b,3}	3.7 (0.7)^{b,3}	3.5 (1.4)^{b,3}	4.0 (1.4)^{b,3}	1.7 (0.7)^{c,3}
VvO	82.2 (0.8)^{a,2}	79.0 (1.6)^{b,1}	77.6 (2.2)^{b,1}	77.4 (2.1)^{b,1}	76.4 (2.5)^{b,1}	77.4 (1.1)^{b,2}
60 days						
VvFb	14.4 (0.7)^{a,3}	20.0 (1.8)^{b,3}	21.5 (0.7)^{b,3}	21.1 (1.1)^{b,4}	21.6 (1.1)^{b,4}	25.5 (2.8)^{c,4}
VvIC	3.9 (0.1)^{a,4}	1.7 (1.5)^{b,4}	2.2 (0.7)^{b,4}	1.9 (0.1)^{b,4}	2.4 (0.4)^{b,4}	0.7 (0.7)^{c,4}
VvO	81.7 (0.7)^{a,2}	78.3 (0.5)^{b,1}	76.3 (2.5)^{b,1}	77.0 (2.4)^{b,1}	76.0 (1.1)^{b,1}	73.8 (1.5)^{b,3}

Mean (standard deviation). The comparison between the groups ($P \leq 0.05$) is indicated by superscript letters (a, b, c) in the various lines. The comparison between the periods ($P \leq 0.05$) is indicated by superscript numbers in the columns.

be used as a root-end filling material (Camilleri *et al.* 2011, Cutajar *et al.* 2011). Recently, it was proposed that the addition of 30% ZrO_2 to the CS provided a material with a radiopacity of approximately 4.12 mm Al (Silva *et al.* 2014). Although it has been reported that the addition of 30% Nb_2O_5 to the CS provides a lower radiopacity than ZrO_2, the average values were approximately 3.52 mm Al (CS + Nb_2O_5micro) and 3.75 mm Al (CS + Nb_2O_5nano) (Silva *et al.* 2015), which are superior to the minimum value recommended for dental materials (Cutajar *et al.* 2011). In addition to the appropriate radiopacity, CS + ZrO_2 and CS + Nb_2O_5 had satisfactory physicochemical and biological properties, and therefore, ZrO_2 and/or Nb_2O_5 are indicated as suitable alternatives for the development of calcium silicate-based materials (Silva *et al.* 2014, 2015, Viapiana *et al.* 2014).

The large number of fibroblasts associated with low number of inflammatory cells observed in the capsules of CS + ZrO_2 and CS + Nb_2O_5 groups clearly suggests that CS + ZrO_2 and CS + Nb_2O_5 promote decreased tissue damage in comparison with MTA Angelus. It is widely reported that bismuth oxide (Bi_2O_3), a radiopacifying agent used in MTA Angelus, may be responsible at least in part for the deleterious effect on tissues (Camilleri *et al.* 2004, Silva *et al.* 2015). Moreover, the recruitment of inflammatory cells also occurs due to the high alkaline pH (pH 11.0) exhibited by calcium silicate-based materials, mainly in the initial periods from 3 h to 7 days (Vosoughhosseini *et al.* 2008, Shahi *et al.* 2010, da Silva *et al.* 2011, Viola *et al.* 2012, Silva *et al.* 2015, da Fonseca *et al.* 2016). In addition to a mild inflammatory reaction, it is expected that a biocompatible material can stimulate the host cells to release cytokines and growth factors, promoting the proliferation of resident cells and consequently allowing the tissues to recover their structural organization.

Amongst several cytokines and growth factors, the FGF family members stimulate cell migration and differentiation, act as cell survival factors and participate in tissue remodelling (Burgess & Maciag 1989, Basilico & Moscatelli 1992, Barrientos *et al.* 2008). FGF-1, a member of the FGF superfamily, is produced by fibroblasts, endothelial cells, inflammatory cells and mast cells (Itoh & Ornitz 2004, Rossini *et al.* 2005, Zakrzewska *et al.* 2008). In adult tissues, FGF-1 is often expressed at sites of inflammatory diseases such as rheumatoid arthritis (Sano *et al.* 1990, 1993, Remmers *et al.* 1991, Byrd *et al.* 1999), inflammatory renal diseases (Rossini *et al.* 2005) and at sites of injury at different phases of the wound healing process (Itoh & Ornitz 2004, Zakrzewska *et al.* 2008, Beenken & Mohammadi 2009).

In the present study, FGF-1 was immunohistochemically detected in the capsules of all the groups. However, a distinct pattern of FGF-1 immunolabelling was detected in the capsules of the experimental material and MTA groups. Considering that a high level of

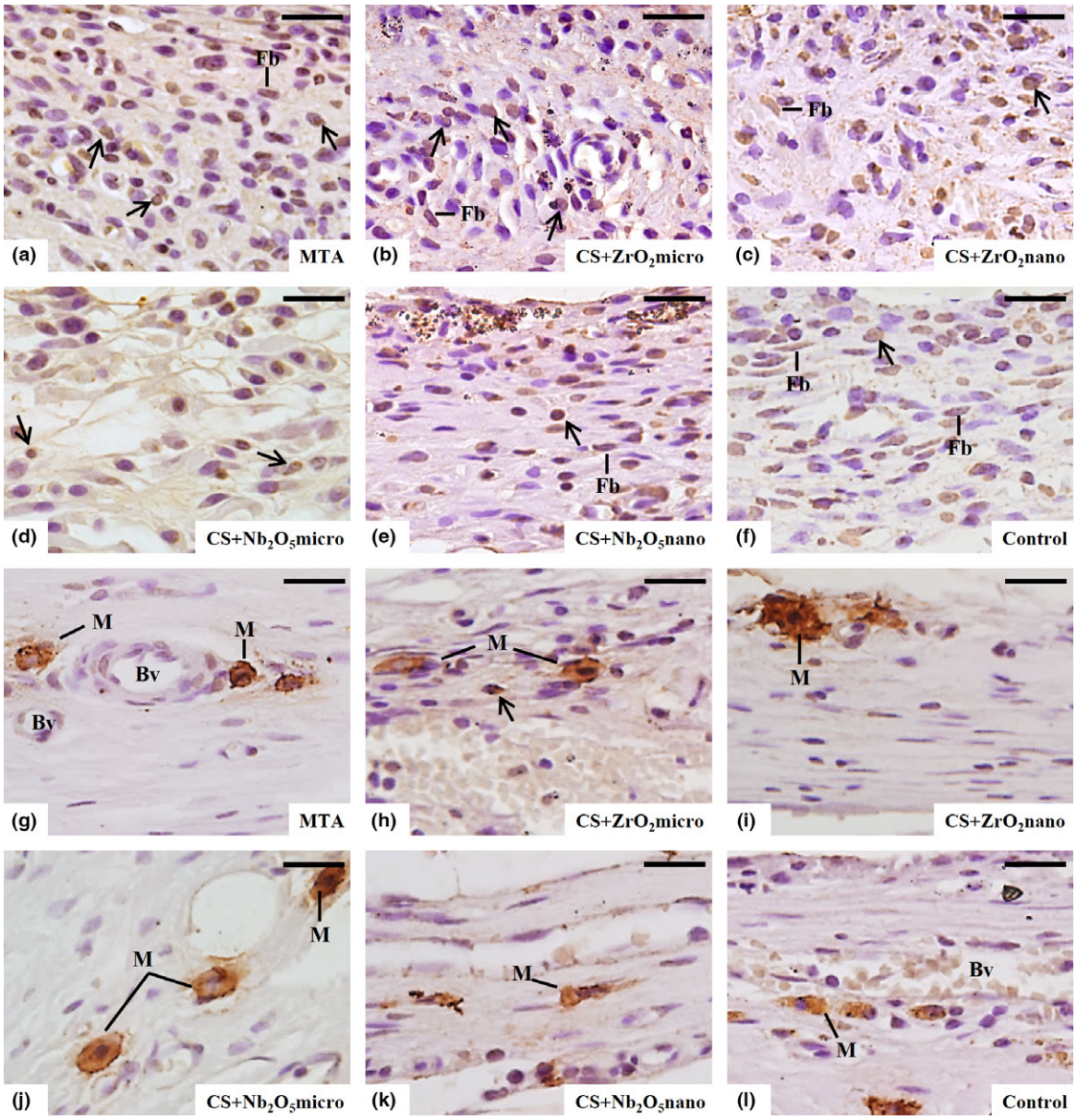

Figure 3 Light micrographs of sections showing portions of the capsules adjacent to the opening of the subcutaneously implanted tubes after 7 (a–f) and 60 (g–l) days of implantation. The sections were subjected to immunohistochemistry for the detection of FGF-1 and were counterstained with haematoxylin. Immunolabelled cells (brown/yellow colour) are observed in the capsules. Arrows, immunolabelled inflammatory cells; Fb, immunolabelled fibroblasts; M, mast cells; Bv, blood vessels. Bars: 20 μm.

FGF in the initial inflammatory reaction induces angiogenesis, an important event in granulation tissue formation (Barrientos *et al.* 2008, Zhao *et al.* 2011), the findings suggest that this factor may induce endothelial cell proliferation, culminating in the presence of several blood vessel profiles, which were often observed in the capsules in the initial periods. Clear immunolabelling was observed in the fibroblasts and inflammatory cells, including lymphocytes, macrophages, plasma cells and mast cells, in the capsules of the all groups. FGF-1 immunoexpression in these cells has been described in several

Table 2 Frequency (%) of birefringent collagen content (Col) and the number of FGF-1 immunolabelled cells per mm^2 in the capsules from the groups after 7, 15, 30 and 60 days

	MTA	CS + ZrO_2 micro	CS + ZrO_2 nano	CS + Nb_2O_5 micro	CS + Nb_2O_5 nano	Control
7 days						
FGF-1	411.1 (17.6)^{a,1}	671.1 (18.1)^{b,1}	635.5 (21.4)^{b,1}	577.7 (20.1)^{c,1}	535.5 (24.0)^{c,1}	868.8 (44.5)^{d,1}
Col	8.7 (0.8)^{a,1}	10.3 (1.2)^{b,1}	9.8 (0.9)^{b,1}	9.9 (2.1)^{b,1}	9.9 (1.3)^{b,1}	13.1 (1.5)^{c,1}
15 days						
FGF-1	222.2 (17.5)^{a,2}	260.0 (6.7)^{b,2}	266.6 (4.4)^{b,2}	266.6 (9.2)^{b,2}	286.6 (14.4)^{c,2}	428.8 (25.5)^{d,2}
Col	9.4 (0.2)^{a,1}	10.2 (2.1)^{b,1}	10.7 (1.4)^{b,1}	10.1 (1.9)^{b,1}	10.4 (1.6)^{b,1}	14.1 (2.5)^{c,1}
30 days						
FGF-1	97.7 (12.1)^{a,3}	176.6 (7.8)^{b,3}	177.7 (26.0)^{b,3}	188.8 (19.0)^{b,3}	103.3 (13.7)^{a,3}	177.7 (12.3)^{b,3}
Col	9.6 (2.5)^{a,1}	11.2 (0.5)^{b,1}	12.6 (2.7)^{b,1}	10.2 (0.1)^{b,1}	12.1 (0.8)^{b,2}	17.7 (0.4)^{c,2}
60 days						
FGF-1	62.2 (5.1)^{a,4}	78.4 (1.8)^{b,4} 23.3	77.7 (3.5)^{b,4}	76.6 (1.6)^{b,4}	73.3 (4.9)^{b,4}	128.8 (16.8)^{c,4}
Col	16.2 (1.2)^{a,2}	(4.5)^{b,2}	23.1 (1.9)^{b,2}	23.7 (1.7)^{b,2}	24.6 (5.4)^{b,3}	34.6 (1.3)^{c,3}

Mean (standard deviation). The comparison between the groups ($P \leq 0.05$) is indicated by different superscript letters (a, b, c) in the various lines. The comparison between the periods ($P \leq 0.05$) is indicated by superscripts numbers in the columns.

tissues and organs (Itoh & Ornitz 2004, Beenken & Mohammadi 2009, Zhao *et al.* 2011, Teven *et al.* 2014). Mast cells produce several cytokines and growth factors that participate in the repair process and wound healing (Norrby 2002, Barrientos *et al.* 2008). Thus, the presence of immunolabelled mast cells strongly suggests that these cells are involved in collagen capsule formation in response to the materials implanted subcutaneously. This hypothesis is supported by the presence of numerous immunolabelled mast cells in the collagen-rich capsules after 60 days.

In addition, the higher FGF-1 immunoexpression may also explain the gradual and significant increase in the incidence of fibroblasts, as FGF-1 plays an important role in fibroblast proliferation (Powers *et al.* 2000, Itoh & Ornitz 2004, Zakrzewska *et al.* 2008). An enhanced FGF-1 immunoexpression is also associated with renal fibrosis (Rossini *et al.* 2005), suggesting that FGF-1 may stimulate collagen synthesis. In the present study, the highest number of FGF-1-immunolabelled cells was accompanied by a high incidence of fibroblasts and increased collagen content in the capsules of the Control group at all time-points. Thus, it is conceivable to suggest that high FGF-1 immunoexpression may promote collagen formation.

The increase in the number of fibroblasts was accompanied by a gradual and significant increase in the birefringent collagen content detected in the capsules over time. This increase in collagen content was associated with the higher number of fibroblasts and a significant reduction in the number of inflammatory cells, which was observed in all the groups, indicating that the materials analysed are biocompatible. However, the experimental materials induced the formation of capsules with a high number of fibroblasts and higher collagen content than in MTA group. Moreover, the capsules juxtaposed to MTA showed an incidence of inflammatory cells that was significantly higher than that of the capsules adjacent to the CS + ZrO_2 and CS + Nb_2O_5 materials. These findings indicate that CS + ZrO_2 and CS + Nb_2O_5 may stimulate cytokine and growth factor release by the host cells. These released molecules are favourable to the proliferation of fibroblasts, which are the cells responsible for the synthesis of extracellular matrix components, allowing the fibrous capsule to form more quickly in comparison with the MTA. The immunohistochemical findings indicate that FGF-1 may play an important role in the complex cascade of cellular events involved in the regression of the inflammatory reaction and fibroblast proliferation. This concept is reinforced by the significant reduction in FGF-1 immunoexpression that was accompanied by decreased collagen content in the MTA group. These findings are consistent with previous studies, which have demonstrated that bismuth oxide, the radiopacifier of MTA, interferes in the biocompatibility of this tricalcium silicate material (Camilleri *et al.* 2004, Silva *et al.* 2015).

There is evidence that particle size interferes in the physicochemical and biological properties of the materials (Wang *et al.* 2007, Xie *et al.* 2013). Nanoparticles added to the CS improve the physicochemical and biological properties of this biomaterial (Saghiri *et al.* 2012, 2015). It was demonstrated that MTA manufactured with small particle components induces a

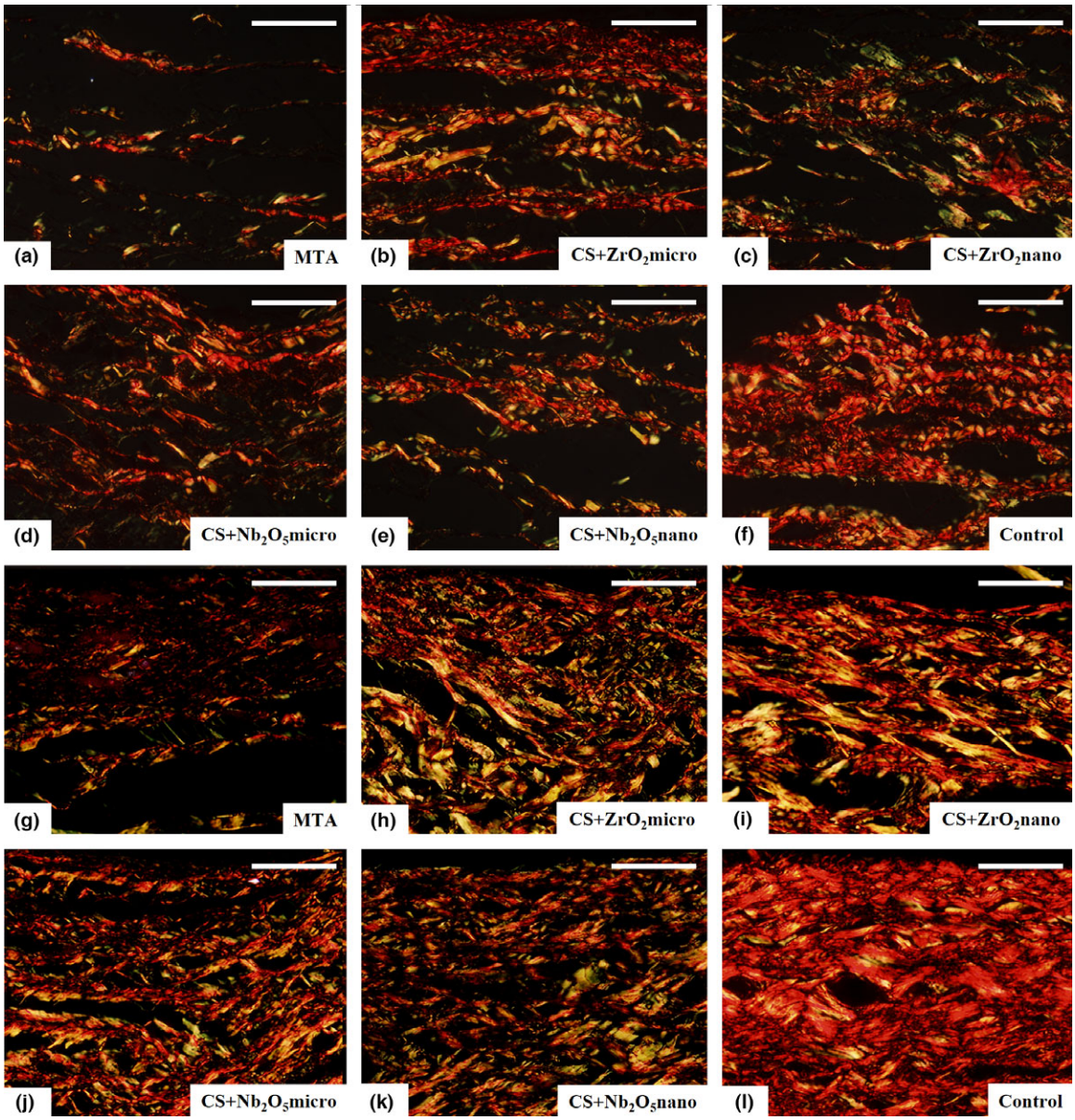

Figure 4 Light micrographs of sections showing portions of the capsules adjacent to the opening of the subcutaneously implanted tubes after 7 (a–f) and 60 (g–l) days of implantation. The sections were subjected to the Picrosirius-red method and analysed under polarized light. An evident increase in the birefringent collagen content (red, yellow and green colours) is observed in the capsules after 60 days in comparison with the period of 7 days. Bars: 40 μm.

lower inflammatory reaction than MTA-Angelus (Saghiri *et al.* 2015). In contrast, the present study shows that nanoparticles of ZrO_2 and Nb_2O_5 do not improve the physicochemical and biological properties of the calcium silicate-based material when compared to microparticulated ZrO_2 or Nb_2O_5 (Silva *et al.* 2014, 2015). In the present study, the findings revealed that CS + ZrO_2nano and CS + Nb_2O_5nano promoted better tissue responses than MTA Angelus.

Conclusions

A calcium silicate-based material associated with zirconium oxide or niobium oxide induced fibroblast

proliferation and accelerated the regression of the inflammatory reaction when compared to MTA Angelus, indicating that ZrO_2 and Nb_2O_5 may be useful alternative radiopacifiers to bismuth oxide. Furthermore, the addition of a nanoparticulate radiopacifier (ZrO_2 and Nb_2O_5) did not improve the biological properties of a calcium silicate-based cement when compared to microparticulate agents.

Acknowledgements

The authors thank Mr. Luis Antônio Potenza and Mr. Pedro Sérgio Simões for kind help and technical assistance. We thank CAPES (Brazil) for the fellowship grant to Guilherme Ferreira da Silva and FAPEAM (Brazil) for fellowship grant awarded to Tiago S. da Fonseca. This study was supported by FUNDUNESP (Proc. no 01054/11-DFP), CNPq (Brazil) and PROPe/PROPG-UNESP (Proc. no 1349).

Conflict of interest

The authors deny any conflict to interests to this study.

References

Barrientos S, Stojadinovic O, Golinko MS, Brem H, Tomic-Canic M (2008) Growth factors and cytokines in wound healing. *Wound Repair and Regeneration* **16**, 585–601.

Basilico C, Moscatelli D (1992) The FGF family of growth factors and oncogenes. *Advances in Cancer Research* **59**, 115–65.

Beenken A, Mohammadi M (2009) The FGF family: biology, pathophysiology and therapy. *Nature Reviews Drug Discovery* **8**, 235–53.

Bortoluzzi EA, Guerreiro-Tanomaru JM, Tanomaru-Filho M, Duarte MAH (2009) Radiographic effect of different radiopacifiers on a potential retrograde filling material. *Oral Surgery Oral Medicine Oral Pathology Oral Radiology and Endodontics* **108**, 628–32.

Burgess WH, Maciag T (1989) The heparin-binding (fibroblast) growth factor family of proteins. *Annual Review of Biochemistry* **58**, 575–606.

Byrd VM, Ballard DW, Miller GG, Thomas JW (1999) Fibroblast growth factor-1 (FGF-1) enhances IL-2 production and nuclear translocation of NF-kappaB in FGF receptor-bearing Jurkat T cells. *Journal of Immunology* **162**, 5853–9.

Camilleri J (2008) The physical properties of accelerated Portland cement for endodontic use. *International Endodontic Journal* **41**, 151–7.

Camilleri J, Montesin FE, Papaioannou S, McDonald F, Pitt Ford TR (2004) Biocompatibility of two commercial forms of mineral trioxide aggregate. *International Endodontic Journal* **37**, 699–704.

Camilleri J, Montesin FE, Di Silvio L, Pitt-Ford TR (2005) The chemical constitution and biocompatibility of accelerated Portland cement for endodontic use. *International Endodontic Journal* **38**, 834–42.

Camilleri J, Cuttajar A, Mallia B (2011) Hydration characteristics of zirconium oxide replaced Portland cement for use as a root-end filling material. *Dental Materials* **27**, 845–54.

Coomaraswamy KS, Lumley PJ, Hofmann MP (2007) Effect of bismuth oxide radioopacifier content on the material properties of an endodontic Portland cement–based (MTA-like) system. *Journal of Endodontics* **33**, 295–8.

Cutajar A, Mallia B, Abela S, Camilleri J (2011) Replacement of radiopacifier in mineral trioxide aggregate; characterization and determination of physical properties. *Dental Materials* **27**, 879–91.

da Fonseca TS, da Silva GF, Tanomaru-Filho M, Sasso-Cerri E, Guerreiro-Tanomaru JM, Cerri PS (2016) In vivo evaluation of the inflammatory response and IL-6 immunoexpression promoted by Biodentine and MTA Angelus. *International Endodontic Journal* **49**, 145–53.

Gandolfi MG, Siboni F, Botero T, Bossù M, Riccitiello F, Prati C (2015) Calcium silicate and calcium hydroxide materials for pulp capping: biointeractivity, porosity, solubility and bioactivity of current formulations. *Journal of Applied Biomaterials & Functional Materials* **13**, 43–60.

Gomes-Cornélio AL, Rodrigues EM, Salles LP *et al.* (2017) Bioactivity of MTA Plus, Biodentine and an experimental calcium silicate-based cement on human osteoblast-like cells. *International Endodontic Journal* **50**, 39–47.

Guerreiro-Tanomaru JM, Storto I, da Silva GF *et al.* (2014) Radiopacity, pH and antimicrobial activity of Portland cement associated with micro- and nanoparticles of zirconium oxide and niobium oxide. *Dental Materials Journal* **33**, 466–70.

Hungaro Duarte MA, Minotti PG, Rodrigues CT *et al.* (2012) Effect of different radiopacifying agents on the physicochemical properties of white Portland cement and white mineral trioxide aggregate. *Journal of Endodontics* **38**, 394–7.

ISO-10993-6 (2007) *Biological Evaluation of Medical Devices-Part 6: Tests for Local Effects After Implantation*. Switzerland: International Standards Organization, pp 1–21.

Itoh N, Ornitz DM (2004) Evolution of the Fgf and Fgfr gene families. *Trends in Genetics* **20**, 563–9.

Junqueira LC, Bignolas G, Brentani RR (1979) Picrosirius staining plus polarization microscopy, a specific method for collagen detection in tissue sections. *Histochemistry Journal* **11**, 447–55.

Junqueira LC, Montes GS, Sanchez EM (1982) The influence of tissue section thickness on the study of collagen by the Picrosirius-polarization method. *Histochemistry* **74**, 153–6.

Koshimizu JY, Beltrame FL, Pizzol JP Jr, Cerri PS, Caneguim BH, Sasso-Cerri E (2013) NF-kB overexpression and

decreased immunoexpression of AR in the muscular layer is related to structural damages and apoptosis in cimetidine-treated rat vas deferens. *Reproductive Biology and Endocrinology* **11**, 29–000. https://doi.org/10.1186/1477-7827-11-29.

Leitune VC, Collares FM, Takimi A *et al.* (2013) Niobium pentoxide as a novel filler for dental adhesive resin. *Journal of Dentistry* **41**, 106–13.

Manni ML, Czajka CA, Oury TD, Gilbert TW (2011) Extracellular matrix powder protects against bleomycin-induced pulmonary fibrosis. *Tissue Engineering Part A* **17**, 2795–804.

Marciano MA, Duarte MA, Camilleri J (2015) Dental discoloration caused by bismuth oxide in MTA in the presence of sodium hypochlorite. *Clinical Oral Investigations* **19**, 2201–9.

Marconyak LJ Jr, Kirkpatrick TC, Roberts HW *et al.* (2016) A Comparison of coronal tooth discoloration elicited by various endodontic reparative materials. *Journal of Endodontics* **42**, 470–3.

Mestieri LB, Tanomaru-Filho M, Gomes-Cornélio AL, Salles LP, Bernardi MIB, Guerreiro-Tanomaru JM (2014) Radiopacity and cytotoxicity of Portland cement associated with niobium oxide micro and nanoparticles. *Journal of Applied Oral Science* **22**, 554–9.

Mitchell PJC, Pitt Ford TR, Torabinejad M, McDonald F (1999) Osteoblast biocompatibility of mineral trioxide aggregate. *Biomaterials* **20**, 167–73.

Norrby K (2002) Mast cells and angiogenesis. *APMIS* **110**, 355–71.

Parirokh M, Torabinejad M (2010) Mineral trioxide aggregate: a comprehensive literature review–Part III: clinical applications, drawbacks, and mechanism of action. *Journal of Endodontics* **36**, 400–13.

Powers CJ, McLeskey SW, Wellstein A (2000) Fibroblast growth factors, their receptors and signaling. *Endocrine-Related Cancer* **7**, 165–97.

Remmers EF, Sano H, Lafyatis R *et al.* (1991) Production of platelet derived growth factor B chain (PDGF-B/c-Sis) mRNA and immunoreactive PDGF B-like polypeptide by rheumatoid synovium: coexpression with heparin binding acidic fibroblast growth factor-1. *The Journal of Rheumatology* **18**, 7–13.

Rich L, Whittaker P (2005) Collagen and picrosirius red staining: a polarized light assessment of fibrillar hue and spatial distribution. *Brazilian Journal of Morphological Sciences* **22**, 97–104.

Rossini M, Cheunsuchon B, Donnert E *et al.* (2005) Immunolocalization of fibroblast growth factor-1 (FGF-1), its receptor (FGFR-1), and fibroblast-specific protein-1 (FSP-1) in inflammatory renal disease. *Kidney International* **68**, 2621–8.

Saghiri MA, Asgar K, Lotfi M, Garcia-Godoy F (2012) Nanomodification of mineral trioxide aggregate for enhanced physiochemical properties. *International Endodontic Journal* **45**, 979–88.

Saghiri MA, Orangi J, Tanideh N *et al.* (2015) Repair of bone defect by nano-modified white mineral trioxide aggregates in rabbit: a histopathological study. *Medicina Oral, Patología Oral y Cirurgía Bucal* **20**, e525–31.

Sano H, Forough R, Maier JAM *et al.* (1990) Detection of high levels of heparin binding growth factor-1 (acidic fibroblast growth factor) in inflammatory arthritic joints. *The Journal of Cell Biology* **110**, 1417–26.

Sano H, Engleka K, Mathern P *et al.* (1993) Coexpression of phosphotyrosine- containing proteins, platelet-derived growth factor-B, and fibroblast growth factor-1 in situ in synovial tissues of patients with rheumatoid arthritis and Lewis rats with adjuvant or streptococcal cell wall arthritis. *The Journal of Clinical Investigation* **91**, 553–65.

Shahi S, Rahimi S, Yavari HR *et al.* (2010) Effect of mineral trioxide aggregates and Portland cements on inflammatory cells. *Journal of Endodontics* **36**, 899–903.

Silva GF, Bosso R, Ferino RV *et al.* (2014) Microparticulated and nanoparticulated zirconium oxide added to calcium silicate cement: evaluation of physicochemical and biological properties. *Journal of Biomedical Materials Research Part A* **102A**, 4336–45.

Silva GF, Tanomaru-Filho M, Bernardi MI, Guerreiro-Tanomaru JM, Cerri PS (2015) Niobium pentoxide as radiopacifying agent of calcium silicate-based material: evaluation of physicochemical and biological properties. *Clinical Oral Investigations* **19**, 2015–25.

da Silva GF, Guerreiro-Tanomaru JM, Sasso-Cerri E, Tanomaru-Filho M, Cerri PS (2011) Histological and histomorphometrical evaluation of furcation perforations filled with MTA, CPM and ZOE. *International Endodontic Journal* **44**, 100–10.

Teven CM, Farina EM, Rivas J, Reid RR (2014) Fibroblast growth factor (FGF) signaling in development and skeletal diseases. *Genes & Diseases* **1**, 199–213.

Viapiana R, Guerreiro-Tanomaru JM, Hungaro-Duarte MA, Tanomaru-Filho CJ (2014) Chemical characterization and bioactivity of epoxy resin and Portland cement-based sealers with niobium and zirconium oxide radiopacifiers. *Dental Materials* **30**, 1005–20.

Viola NV, Guerreiro-Tanomaru JM, Silva GF, Sasso-Cerri E, Tanomaru-Filho M, Cerri PS (2012) Morphological and morphometric analysis of the biocompatibility of an experimental MTA Sealer. *Journal of Biomedical Materials Research Part B, Applied Biomaterials* **100B**, 1773–81.

Vosoughhosseini S, Lotfi M, Shahi S *et al.* (2008) Influence of white versus gray mineral trioxide aggregate on inflammatory cells. *Journal of Endodontics* **34**, 715–7.

Wang H, Li Y, Zuo Y, Li J, Ma S, Cheng L (2007) Biocompatibility and osteogenesis of biomimetic nano-hydroxyapatite/polyamide composite scaffolds for bone tissue engineering. *Biomaterials* **28**, 3338–48.

Xie KY, Wang Y, Zhao Y *et al.* (2013) Nanocrystalline β-Ti alloy with high hardness, low Young's modulus and excellent in vitro biocompatibility for biomedical applications. *Material Science & Engineering C Materials for Biological Applications* **33**, 3530–6.

Zakrzewska M, Marcinkowska E, Wiedlocha A (2008) FGF-1: from biology through engineering to potential medical applications. *Critical Reviews in Clinical Laboratory Sciences* **45**, 91–135.

Zhao T, Zhao W, Chen Y, Ahokas RA, Sun Y (2011) Acidic and basic fibroblast growth factors involved in cardiac angiogenesis following infarction. *International Journal of Cardiology* **152**, 307–13.

